Haptic Interaction Stability With Respect to Grasp Force

Janez Podobnik and Marko Munih, *Member, IEEE*

***Abstract*—This paper addresses the contact instability of admittance control of a haptic interface. A high level of rigidity of the grasp of a subject operating the haptic interface will result in unstable behavior of the haptic interaction. Experiments with a system dedicated to measuring grasp force were performed to explore the conditions when grasp force has reached the critical grasp force that destabilizes the haptic interface. The critical grasp force was quantified for various values of virtual environment parameters. The experimental results are compared to simulation results obtained with a model of haptic interaction. To improve stability, two methods were applied: one with virtual coupling, the other with a compensator filter. A model was used to define the structure of the compensator filter and to determine the parameters of the virtual coupling and the compensator filter. Experimental and simulation results confirmed an improvement of stability. Both methods allow higher grasp forces of the human operator, and experiments show that the compensator filter allows higher grasp forces than the virtual coupling.**

***Index Terms*—Control systems, haptic interface, human–robot interaction, simulation, stability.**

I. Introduction

HAPTIC interfaces render kinesthetic information to a human operator interacting with a virtual environment [1], [2]. There are two basic embodiments of haptic interfaces: an admittance interface, where forces are measured and motion is displayed [2], and an impedance interface, where motion is measured and forces are displayed [3].

Instability affects the performance of haptic interfaces [1], distorting the interaction with the virtual environment. A haptic interface must be stable for a wide range of admittances/impedances of the virtual environment [4]. The stability of a robot force control depends upon the chosen combination of sampling time and controller gain, and upon the chosen parameters of compliance (relation between position and force) and stiffness of the contacted environment.

Sustained and growing oscillations previously observed by several researchers [1], [5], [6] may appear when a simulated discrete passive virtual environment and a passive human operator are coupled through the haptic interface in a haptic interaction. At admittance type, the instability will occur when the impedance of the subject is high (rigid grasp) and impedance of the virtual environment is low (free space) [5].

Manuscript received October 18, 2005; revised April 18, 2006 and November 29, 2006. This work was supported by the Slovenian Research Agency. This paper was recommended by Associate Editor Z. Wang.

The authors are with the Laboratory of Biomedical Engineering and Robotics, Faculty of Electrical Engineering, University of Ljubljana, SI-1000 Ljubljana, Slovenia (e-mail: janezp@robo.fe.uni-lj.si; marko@robo.fe.uni-lj.si).

Digital Object Identifier 10.1109/TSMCC.2007.905816

Previous experimental work and practice show that grasp can destabilize the haptic interface; however, there has been no report of experiments to determine the influence of grasp on the stability of a haptic interface. In fact, Clover [2] reports that, in general, the haptic interface literature lacks a sufficient number of experimental examples where dynamic force and moment interaction have been considered. Burke *et al*. [7] reports findings of the study on the human–robot interaction that identified major issues to be solved. A major issue is system architecture, which explicitly includes the human in the loop and knowledge acquisition as the foundation of modeling. The main objective of the research presented here is the evaluation of the dependence of instability on the grasp force of the human operator. Observations show that for grasp forces lower than the critical grasp force, the haptic interface will remain stable. When the grasp force has reached the critical value, the haptic interface will become unstable. The transition from the stable to the unstable state is sudden, and is accompanied by pronounced oscillation. Both the critical grasp force (F_c) and the frequency of oscillation can be determined.

Grasp force is correlated with the biomechanical impedance of the grasp [8]; a light grasp corresponds to low impedance (low level of stiffness) and a tight grasp corresponds to high impedance (high level of stiffness) [9]. Stability was studied with respect to the parameters of the virtual environment and, most importantly, with reference to the critical grasp force of the human operator. Contact instability was investigated experimentally with an actual haptic interface and by simulation using a model of haptic interaction with no additional improvement, then with virtual coupling [1], and last with a compensator derived from the proposed model. The compensator is used as a filter of the input force exerted by the human operator. The use of a compensator filter introduces a two-degree-of-freedom (2-DOF) haptic control scheme, where a PV controller is used as a feedback controller, and a compensator filter functions as a feedforward filter for optimizing the response.

The data of an original system and those of improved systems were compared in order to demonstrate the effect of improvements. A comparison of experimental and simulation data shows that the linear control theory can describe the system of a haptic interaction adequately and can predict regions of instability, thus simplifying the analysis of the stability of a haptic interface.

II. Methods

A. Model of A Haptic Interaction

The 1-DOF model of the haptic interaction considered here is given in Fig. 1. The model consists of a human operator, a

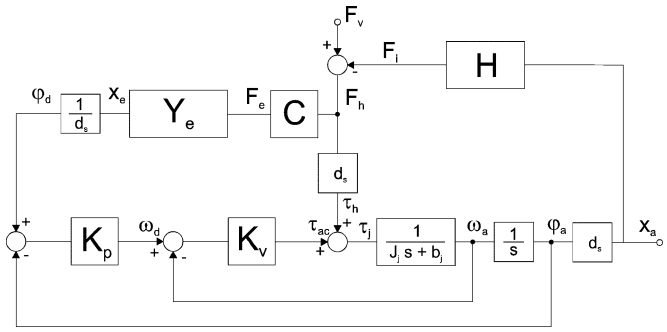

Fig. 1. Model of a 1-DOF haptic interaction. The model includes a human operator, a virtual environment, and an one-segment admittance haptic display.

virtual environment, and a one DOF admittance haptic display. The force F_h applied by the human operator is the sum of voluntary force F_v and intrinsic force F_i. Bennett *et al*. [10] measured the human arm joint inertia $J_{\rm ha} = 0.072\ \mathrm{N{\cdot}ms^2{\cdot}rad^{-1}}$ and damping $b_{\rm ha} = 0.62\ \mathrm{N{\cdot}ms{\cdot}rad^{-1}}$. Comparison of values for the human arm joint with those for the robot arm joint shows that the robot arm joint inertia is 38 times larger than of the human arm joint, while the robot arm damping is 11 times larger than that of the human arm joint (see Table II for robot arm joint inertia J and damping b). The robot arm dynamics thus prevails over those of the human arm dynamics, and thus can be modeled as linearized endpoint stiffness $H(s) = K$ [11]. The assumption is made that the human operator is passive [3]. The input force F_e in the virtual environment Y_e is force F_h filtered with prefilter C. The torque τ_j is the sum of controller torque $\tau_{\rm ac}$ and torque τ_h exerted by the human operator ($\tau_h = d_s F_h$, d_s is the length of the segment). Angle φ_d is the desired angle, x_e is the desired position ($\varphi_d = \frac{1}{d_s} x_e$), x_a is the actual position, and φ_a is the actual angle ($x_a = d_s \varphi_a$). The admittance of the virtual environment Y_e consists of virtual mass m_e, virtual damping b_e, and virtual stiffness k_e in the following form:

$$Y_e = \frac{1}{m_e s^2 + b_e s + k_e}. \tag{1}$$

The transfer function $\widehat{Y}_e$ conveys the state felt by the operator as endpoint admittance for the given virtual environment Y_e

$$\widehat{Y}_e(s) = \frac{d_s^2 + K_v K_p C Y_e}{Z_j s + K_v s + K_v K_p} \tag{2}$$

$$= \frac{d_s^2}{Z_j s + K_v s + K_v K_p} + H_i C Y_e \tag{3}$$

where

$$H_i(s) = \frac{K_v K_p}{Z_j s + K_v s + K_v K_p}.$$

Here, K_p and K_v are PV controller gains, Z_j represents the manipulator joint dynamics ($Z_j = Js + b$, J is joint inertia, b is joint damping), and d_s is the segment length (see Table II for numeric values). Prefilter $C(s)$ is included in the model and discussed in detail in Section II-D. The sampling time is 250 μs, the time constants of the model are greater than 10 ms, and, thus, the effects of the sample and hold can be omitted [12].

The first part of (3) represents a mechanical coupling between the human operator and the mechanical structure of the haptic display. The second part of (3) is the admittance of the virtual environment mapped through $H_i(s)$, which is a model of a one-segment admittance haptic display consisting of a cascade of the PV controller and manipulator joint dynamics Z_j.

The minimum endpoint admittance that the haptic interface can simulate is as follows:

$$\widehat{Y}_{e,\min}(s) = \widehat{Y}_e(s)|_{Y_e \to 0} = \frac{d_s^2}{Z_j s + K_v s + K_v K_p}. \tag{4}$$

$Y_e \to 0$ is achieved with very high values of the parameters of the virtual environment ($m_e \to \infty$, $b_e \to \infty$, and $k_e \to \infty$; high inertia, highly damped, and very stiff environment, which is the opposite of free space). The minimum admittance of the virtual environment will be affected by the mechanical coupling between the human operator and the mechanical structure of the haptic display. The maximum endpoint admittance to be simulated by the haptic interface is as follows:

$$\widehat{Y}_{e,\max}(s) = \widehat{Y}_e(s)|_{Y_e \to \infty} \to \infty \tag{5}$$

whereby the admittance haptic interface can simulate an arbitrary low impedance $Z_e = 1/Y_e$ of free space. Simulating an arbitrary low impedance of free space with an actual admittance type haptic interface is limited by the stability of the haptic interaction. The transparency of free space will be affected by the function $H_i(s)C(s)$, which consists of joint and PV controller dynamics, and of the compensator filter (discussed later).

Instability will occur when the admittance of the virtual environment Y_e is high [5], which corresponds to the low impedance $Z_e = 1/Y_e$ of free space. Also, the PV controller gain parameters K_v and K_p are high, which is usual for such an application [11]. Since the work envelope (workspace) of a manipulator is less than 1 $\mathrm{m}(d_s^2 < 1)$ the $K_v K_p C Y_e$ part of (2) thus prevails over the d_s^2 part of (2), and (3) can be simplified for the purpose of studying the stability of the haptic interaction. By adding a representation of the human operator $H(s) = K$, the full open-loop transfer function $\widehat{Y}_e(s)H(s)$ becomes

$$\widehat{Y}_e(s)H(s) = K \frac{K_v K_p C Y_e}{Z_j s + K_v s + K_v K_p} = K H_i C Y_e. \tag{6}$$

The closed-loop transfer function is as follows:

$$x_a = \frac{\widehat{Y}_e(s)}{1 + \widehat{Y}_e(s)H(s)} F_v \tag{7}$$

where x_a is the actual endpoint position of the haptic interface and F_v is the voluntary force exerted by the human operator. $\widehat{Y}_e(s)$ is in the forward path, and the transfer function $H(s)$ is in the feedback path.

B. Equipment

A general-purpose haptic interface with an industrial Stäubli RX90 robot was used in this study. The haptic interface was developed to display a wide range of impedances for arm-size haptic interactions. The architecture of the controller allows

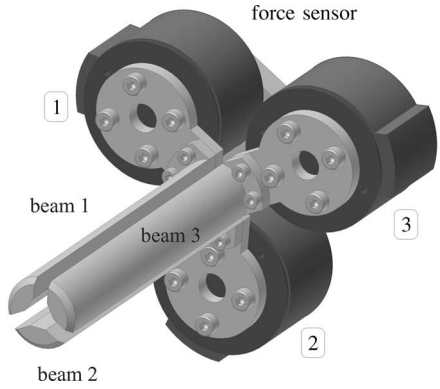

Fig. 2. Grasp force-measuring system. Beam 1 is attached to the force-torque sensor 1, beam 2 to the sensor 2, and beam 3 to the sensor 3.

the design of a custom-made robot controller with a personal computer (PC). The controller is implemented on RTlinux with 4-kHz sampling loop frequency.

C. Measurement Equipment

A grasp force-measuring handle was designed to evaluate the influence of the human operator on the stability of the haptic interaction (see Fig. 2). The handle is split into three beams, and each beam is attached to a separate JR3 force-torque sensor, which allows a wide measuring range of grasp force (0–260 N). The symmetrical arrangement of the three beams allows us to quantify grasp force independently of the position of the hand [13]. For each beam, the radial and the tangential force on the beam are calculated from the xy forces given by the corresponding sensor. This was realized by transforming force-torque Cartesian space data from each sensor into a cylindrical coordinate system aligned with the axis of the handle. The radial components of each beam are then summed as the grasp force. An additional force-torque sensor for measuring contact force F_h is attached between the handle force sensors and the top of the robotic manipulator. JR3 force-torque sensors contain analog and digital circuitry; analog data are converted to digital data within the sensor housing. The sensors are connected to JR3 DSP-based force sensor receivers, where force-torque data are filtered with a cutoff frequency of 125 Hz. The hand grasp force measuring system is sufficiently robust to operate in specific conditions of invoked instability.

D. Force-Filtering Compensator Filter

The compensator filter is a feedforward part of the control law framework presented here, and the PV controller is a feedback part of the control law framework. The starting point for deriving the force-filtering compensator filter is the model described with (6). $H_i(s)$ is a model of a one-segment admittance haptic display consisting of a cascade of the PV controller and manipulator joint dynamics Z_j. To achieve stability and good transparency of the haptic interface, $H_i(s)C(s)$ must be close to 1. Since the transfer function $H_i(s)$ is strictly proper (more poles than zeros), $C(s) = 1/H_i(s)$ would be a noncausal filter. To preserve the causality of $C(s)$, the following form is adopted:

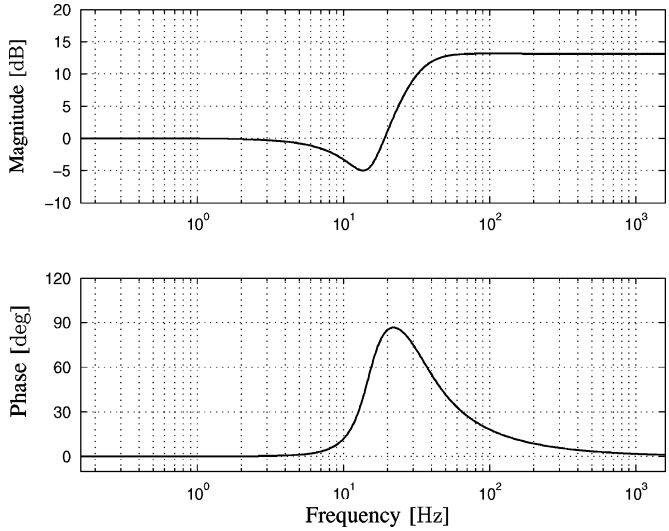

Fig. 3. Bode diagram of the force compensator filter; observe positive phase in the region where the phase margin has to be improved.

$$C(S) = \frac{\omega_c^2}{\frac{K_v K_p}{J}} \frac{s^2 + \frac{K_v + b}{J}s + \frac{K_v K_p}{J}}{s^2 + 2\zeta_c\omega_c s + \omega_c^2} = \frac{\omega_c^2}{\omega_h^2} \frac{s^2 + 2\zeta_h\omega_h s + \omega_h^2}{s^2 + 2\zeta_c\omega_c s + \omega_c^2} \tag{8}$$

where ω_c determines the new bandwidth of the modeled haptic interface. ω_c should be chosen to be greater than the time constants of $H_i(s)$, and then $H_i(s)C(s) \approx 1$ for $\omega < \omega_c$, which improves the overall transparency of the haptic interface. $H_i(s)C(s)$ takes the following form:

$$H_i(s)C(s) = \frac{\omega_c^2}{s^2 + 2\zeta_c\omega_c s + \omega_c^2}. \tag{9}$$

The minimum and maximum endpoint admittances and, thus, the Z-width for the haptic interface with a compensator filter, do not change. Fig. 3 shows a Bode diagram of force filter $C(s)$. The positive angle phase of filter $C(s)$ raises the overall curve of the angle phase, and increased damping moves unstable poles into the left-half complex plane, thus improving stability. The amount of high-frequency attenuation depends upon the ratio between the denominator and numerator bandwidths.

E. Virtual Coupling

This section gives a general insight into the virtual coupling; a full and detailed description is given in [1]. The design of the implemented virtual coupling follows exactly the design given in [1]

$$Z_c = \frac{1}{\frac{1}{b_c} + \frac{1}{m_c s}} = \frac{m_c b_c s}{m_c s + b_c} \tag{10}$$

$$F_e = F_h - Z_c v_e = F_h - Z_c s x_e. \tag{11}$$

Equation (10) gives the impedance function of virtual coupling, while (11) gives the control law. Function $\widehat{Y}_e(s)$ becomes

$$\widehat{Y}_e(s) = \frac{d_s^2}{Z_j s + K_v s + K_v K_p} + H_i \frac{Y_e}{1 + Z_c s\, Y_e}. \qquad (12)$$

The minimum endpoint admittance that the haptic interface with virtual coupling can simulate is not affected, while the maximum endpoint admittance that a haptic interface with virtual coupling can simulate is affected

$$\widehat{Y}_{e,\max}(s) = \widehat{Y}_e(s)|_{Y_e \to \infty} = \frac{d_s^2}{Z_j s + K_v s + K_v K_p} + H_i \frac{1}{Z_c s}. \qquad (13)$$

Thus, virtual coupling will affect the Z-width of the admittance haptic display [1].

F. Experimental Protocol

A series of experiments was conducted for each of the parameters of the virtual environment (m_e, b_e, and k_e). In each series, one of the virtual environment parameters was independently variable, while the other two parameters were fixed at reference values. The experiments can be classified as follows.

- Virtual mass series experiments: The virtual environment mass m_e is varied in the range 0.1–1.5 kg, while the other two parameters of the virtual environment are fixed at $b_e = 50\ \frac{\text{Ns}}{\text{m}}$ and $k_e = 0\ \frac{\text{N}}{\text{m}}$.
- Virtual damping series experiments: Damping b_e is varied in the range 2–50 $\frac{\text{Ns}}{\text{m}}$, with fixed values $m_e = 1.5$ kg, $k_e = 0\ \frac{\text{N}}{\text{m}}$.
- Virtual stiffness series experiments: Stiffness k_e is varied in the range 0–150 $\frac{\text{N}}{\text{m}}$, with fixed values $m_e = 1$ kg, $b_e = 40\ \frac{\text{Ns}}{\text{m}}$.

For each combination of the virtual parameter values, the grasp force was increased step by step during the experiment. The value of the grasp force where the system has become marginally stable is the critical grasp force. The size of the grasp force was represented by the height of a blue bar that was projected onto a wide screen. The desired value of the grasp force was indicated with a red line. The online visual feedback information allowed the user to maintain a constant grasp force at the reference value. The subject maintained the grasp force at a reference value represented by a red line, while moving the robot arm with slow movements inside the space with chosen parameters of the virtual environment. Fig. 4 shows the experimental setup. The test lasted 10 s, and provided the haptic interface stayed stable, the robot stopped, giving the signal for saving data from buffer to disk. The robot was then moved back to the starting position and the reference grasp force was raised by 5 N. This procedure was repeated up to levels where the haptic interface became unstable. The grasp force of the subject at the moment of transition from the stable to the unstable state of the haptic interaction was denoted as the critical grasp force F_c. The transition from the stable to the unstable state was sudden, and was accompanied by pronounced oscillations. When F_c for a particular set of values of virtual environment parameters was determined, the independent variable of the virtual environment parameter was increased to the next value of the particular series experiment (see Table I for values of the parameters for which the measurements were performed). At preselected values $b_e = 35\ \frac{\text{Ns}}{\text{m}}$ in compensator mode and $b_e = 45\ \frac{\text{Ns}}{\text{m}}$ in virtual coupling mode, the haptic interface was stable. Instead of preselected values, the highest value of b_e for which the haptic interface was unstable was used in the series.

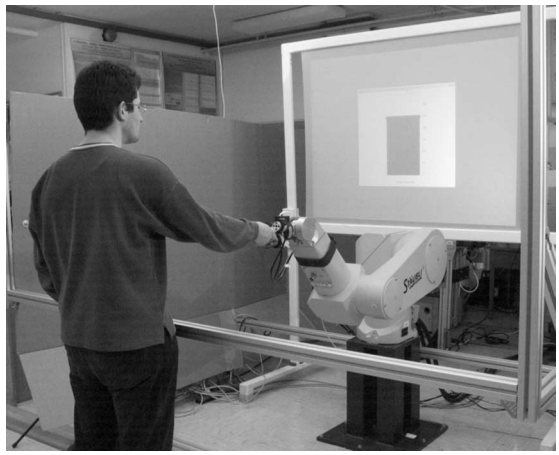

Fig. 4. Experimental setup. In the center is the robot arm of a Stäubli RX90 industrial robot located in the robotic cell. Behind the robot is a bar indicating the size of the grasp force projected on the screen. Subject grasps the grasp force-measuring system.

TABLE I
INCREMENT SERIES OF VIRTUAL ENVIRONMENT PARAMETERS

virtual mass m_e [kg], $b_e = 50\ \frac{\text{Ns}}{\text{m}}$, $k_e = 0\ \frac{\text{N}}{\text{m}}$									
N	0.25	0.50	0.60	0.80	0.90	0.95	1.00	1.20	1.50
C	0.10	0.25	0.50	0.60					
VC	0.10	0.25	0.50	0.75					
virtual damping b_e $[\frac{\text{Ns}}{\text{m}}]$, $m_e = 1.5$ kg, $k_e = 0\ \frac{\text{N}}{\text{m}}$									
N	5	15	20	25	30	35	40	45	50
C	2	5	10	15	20	30	32		
VC	2	5	10	15	20	30	40	42	
virtual stiffness k_e $[\frac{\text{N}}{\text{m}}]$, $m_e = 1$ kg, $b_e = 40\ \frac{\text{Ns}}{\text{m}}$									
N	0	25	50	100	150				

N, normal mode; C, compensator mode; VC, virtual coupling mode

Following the baseline measurements (normal mode) as explained earlier, the compensator filter (compensator mode) and the virtual coupling (virtual coupling mode) were implemented, with the experiments repeated each time. The frequency of oscillation was determined offline with autocorrelation of the recorded endpoint position time series.

To ensure consistent results, the same person participated in all the experiments. In the present case, the subject, a postgraduate student of robotics, was a 24-year-old right-handed male, with no signs of neurological problems. The subject was well acquainted with the haptic interface and the virtual environment. The subject participated in the preliminary experiments and was familiar with the procedures and the interaction. Hence, the assumption was made that the subject's interaction approach did not change during the experiments.

The virtual environment, the compensator filter, and the virtual coupling were implemented as discrete filters derived from

TABLE II
PARAMETERS OF MODEL USED IN SIMULATION, PARAMETERS OF FORCE COMPENSATOR FILTER, AND PARAMETERS OF VIRTUAL COUPLING

J [Nms^2 rad^{-1}]	b [Nms rad^{-1}]	K_p	K_v
2.77	7.00	194.87	126.27
ω_h [rads^{-1}]	ζ_h	ω_c [rads^{-1}]	ζ_c
93.9	0.283	200.0	0.600
m_c [kg]	b_c [Ns m^{-1}]	d_s [m]	
3	550	0.45	

the analog form thereof [(1), (8), and (10)] with bilinear or Tustin transformation in the main real-time control loop. Simulation was performed by Matlab with control system toolbox. Every block of Fig. 1 is implemented as a continuous-time LTI model.

III. RESULTS

A. Model Stability Analysis

Stability was examined with root-locus analysis. Table II gives the values of the parameters used in the simulation and the parameters of the force compensator filter virtual coupling.

The values of the human arm grasp stiffness K, where poles of closed-loop model of haptic interaction became unstable, were calculated, and taken as critical values of human arm stiffness K_c. Figs. 5(a), 6(a), and 7(a) show the values of K_c for uncompensated system [broken line, eq. (6)], for compensated system, and for system with virtual coupling (dotted line). The simulation data presented here show that the overall human arm stiffness K is mostly in the range 1000–10000 $\frac{\mathrm{N}}{\mathrm{m}}$ [see Figs. 5(a), 6(a), and 7(a)]. A plot of the frequency of oscillation was constructed [Figs. 5(a), 6(b), and 7(b)]. The critical value of human arm stiffness K_c and the frequency of oscillation are virtual environment-dependent parameters (m_e, b_e, and k_e). Fig. 8 shows simulation results for high values of stiffness k_e.

B. Experimental Results

Experiments on an actual haptic interface were performed to verify the effects of contact instability. As with the model, experiments were performed with an uncompensated system, a compensated system, and one with virtual coupling.

The critical grasp force F_c is the grasp force of the human operator at the moment of transition from the stable to the unstable state of the haptic interaction. The critical grasp force F_c and the frequency of oscillation are virtual environment-dependent parameters (m_e, b_e, and k_e). Fig. 12 shows the plots of grasp force [Fig. 12(a)] and endpoint position [Fig. 12(b)] in the experimental case of invoked instability.

The measured values for grasp force F_c presented in Figs. 9–11 are expected to vary at the most: for region [5–13] N $\pm$ 2 N, for region [13–50] N $\pm$ 5 N, for region [50–150] N $\pm$ 10 N, and for region above 150 N $\pm$ 20 N. The frequencies presented in Figs. 9–11 are expected to vary upmost for ± 0.41 Hz.

C. Comparison of Simulations and Experiments

A common tendency of F_c and K_c for all three modes [Figs. 5(a) and 9(a)] is that they increase by increasing m_e.

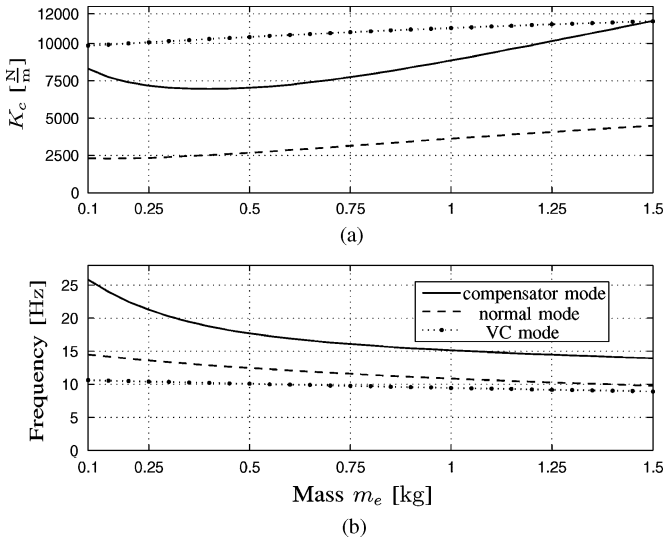

Fig. 5. Results of the stability analysis with the model of haptic interaction (a) K_c and (b) frequency of oscillation with respect to m_e. (Solid line) Compensated system. (Broken line) Uncompensated system. (Dotted line) Virtual coupling.

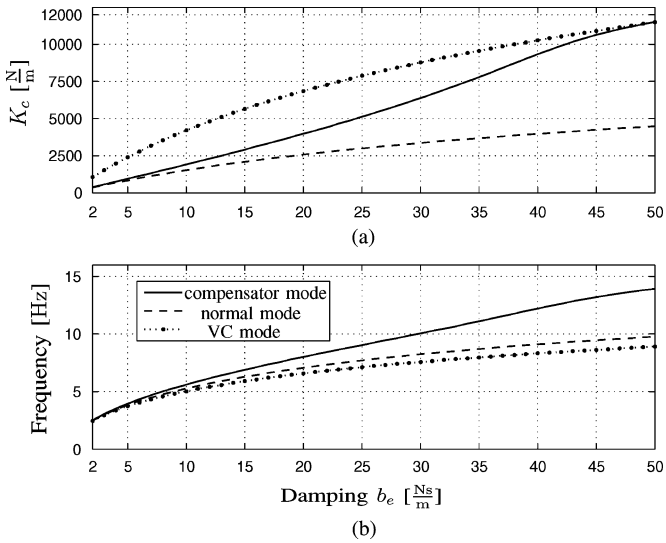

Fig. 6. Results of the stability analysis with the model of haptic interaction (a) K_c and (b) frequency of oscillation with respect to b_e. (Solid line) Compensated system. (Broken line) Uncompensated system. (Dotted line) Virtual coupling.

There is a slight deviation from this rule for the compensated mode in the simulated set, where K_c first decreases, then starts to increase at $m_e = 0.4$ kg by increasing m_e. A comparison of Figs. 5(b) and 9(b) shows a common tendency of the frequency of oscillation for the simulated and the experimental data set. Both decrease by increasing m_e.

There is a discrepancy between the simulation and the experimental results regarding the frequency of oscillation. The simulation results show that the frequency of oscillation of a system with a compensator is much higher than the frequency of oscillation of the system with virtual coupling, while the experimental results show that all frequencies of oscillation of all

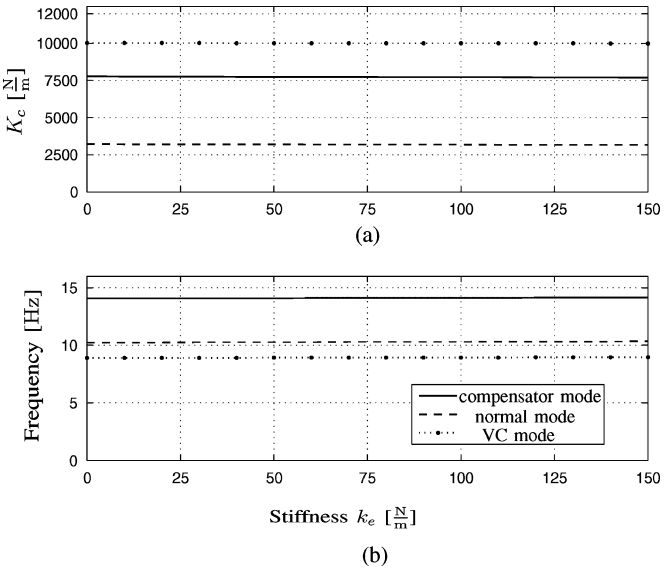

Fig. 7. Results of stability analysis with model of haptic interaction (a) K_c and (b) frequency of oscillation with respect to k_e. (Solid line) Compensated system. (Broken line) Uncompensated system. (Dotted line) Virtual coupling.

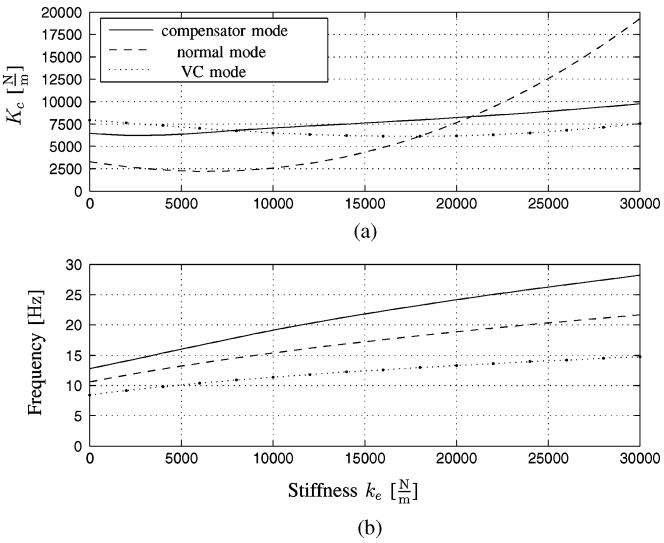

Fig. 8. Results of stability analysis with model of haptic interaction for large k_e (a) K_c and (b) frequency of oscillation with respect to k_e. (Solid line) Compensated system. (Broken line) Uncompensated system. (Dotted line) Virtual coupling.

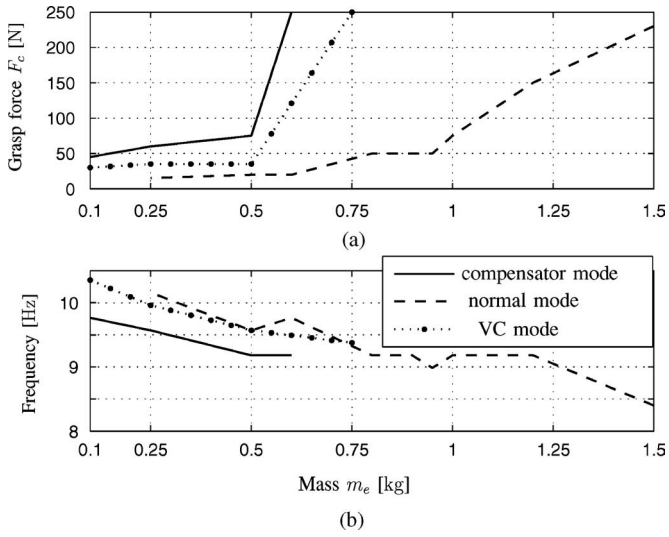

Fig. 9. Experimental results of stability analysis (a) F_c and (b) frequency of oscillation with respect to various values of m_e. (Solid line) Compensator filter. (Broken line) Uncompensated system. (Dotted line) Virtual coupling.

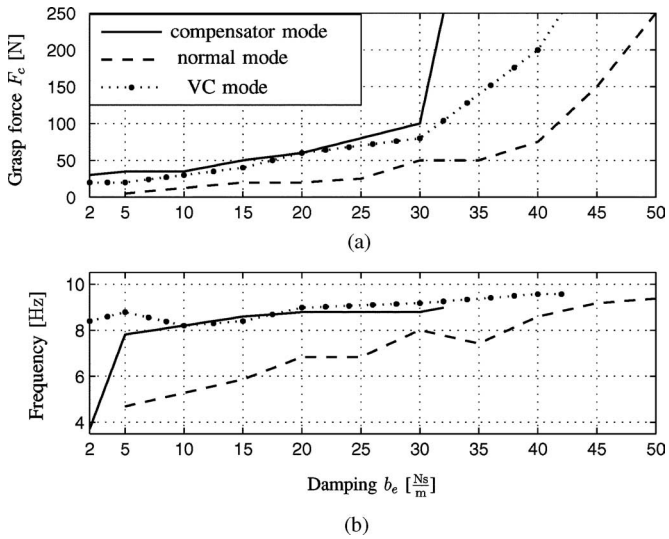

Fig. 10. Experimental results of stability analysis (a) F_c and (b) frequency of oscillation with respect to various values of b_e. (Solid line) Compensator filter. (Broken line) Uncompensated system. (Dotted line) Virtual coupling.

three modes are very similar. The frequencies encountered for the compensated system are higher, which suggests that loci branches of the compensated system are further apart than those of the uncompensated system.

A comparison of Figs. 6 and 10 shows a common tendency of F_c, K_c, and the frequency of oscillation to increase by increasing b_e. A minor deviation from this general trend can be observed for F_c [Fig. 10(b)] as, for instance, the value of the frequency of oscillation for the uncompensated system [Fig. 10(b)] at $b_e = 30\ \frac{\text{Ns}}{\text{m}}$ is higher than the value at $b_e = 35\ \frac{\text{Ns}}{\text{m}}$. A discrepancy similar to that observed in the virtual mass series experiments regarding the frequency of oscillation can be seen in the virtual damping series experiments. For the compensator and virtual coupling modes, the frequencies of oscillation are again similar, while the frequency of oscillation for the normal mode is lower than that of the other two modes.

A comparison of Figs. 11 and 7 shows that K_c, F_c, and the frequency of oscillation are constant for low values of k_e. The general trend is that both grasp force F_c [Fig. 11(a)] and frequency [Fig. 11(b)] remain essentially constant with only minor deviations. Fig. 11 shows the results of experiments with the uncompensated system, while the compensated system and the system with virtual coupling were stable for grasp forces within the range of the measuring equipment (0–260 N).

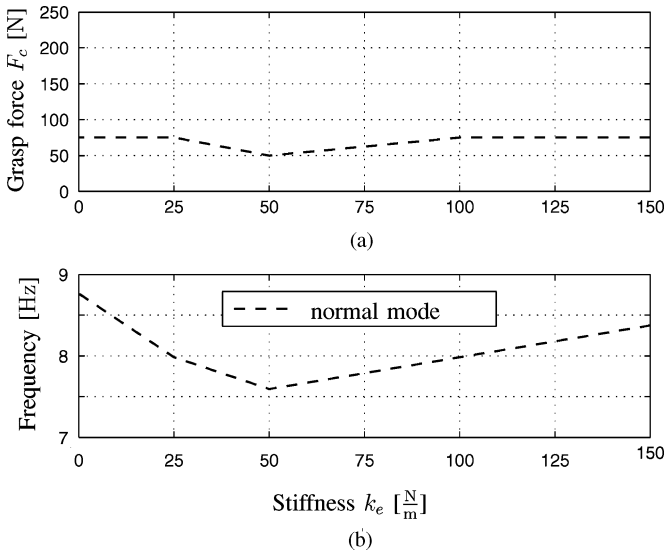

Fig. 11. Experimental results of stability analysis (a) F_c and (b) frequency of oscillation with respect to various values of k_e. (Broken line) Uncompensated system.

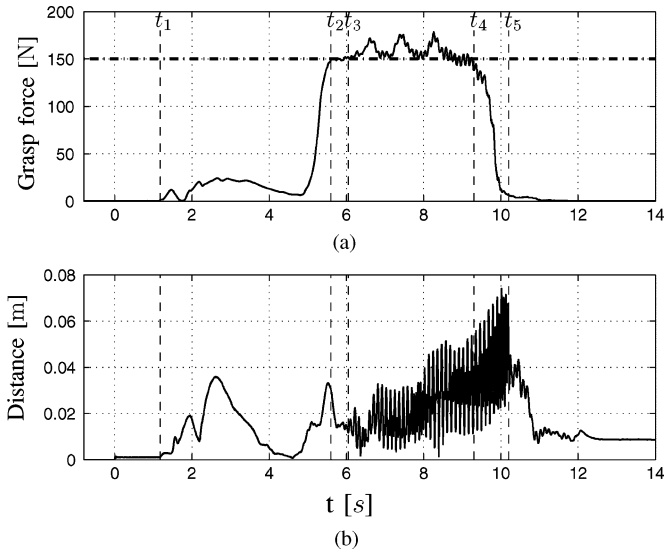

Fig. 12. Experiment where instability was invoked when grasp force reached the critical grasp force $F_c = 150$ N ($m_e = 1.5$ kg, $b_e = 45\ \frac{\text{N s}}{\text{m}}$, $k_e = 0\ \frac{\text{N}}{\text{m}}$, normal mode). At $t_1 = 1.2$ s, subject grasped a handle; at $t_2 = 5.6$ s, the critical grasp force was reached; and, at $t_3 = 6.1$ s, the haptic interface became unstable. At $t_4 = 9.3$ s, the subject started to reduce the grasp force and, at $t_5 = 10.2$ s, the haptic interface became stable again.

IV. Discussion

A. Relation Between the Parameters of Virtual Environment and Stability of the Haptic Interface

The results of simulation suggest that virtual coupling is a better choice than the compensator filter for improving stability, while the experimental results show that a compensator filter gives better results for an actual haptic interface. This suggests that a compensator filter is less susceptible to the differences between the model of the haptic interface and the actual haptic interface. The compensator filter is designed to compensate for the poles introduced by manipulator joint dynamics and the PV controller. The virtual coupling aims to provide unconditional

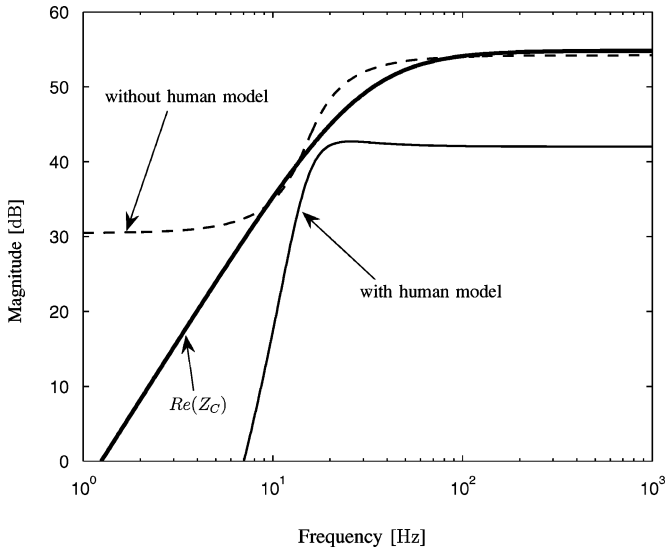

Fig. 13. Llewellyn's stability criteria for admittance haptic display; left side of the Llewellyn's inequality ($Re(Z_C)$, bold line) and right side of the Llewellyn's inequality with (full line) and without (dashed line) human model.

stability of the whole system in terms of Llewellyn's stability criteria in such a way that the Llewellyn's inequality holds [1]. Figs. 5(a), 6(a), and 7(a), dotted line, show the maximum values of the stiffness K for a given human model for which the interaction remains stable. Adams *et al*. state that a conservative design that considers unreasonable levels of human interaction required virtual coupling impedance at excessive levels [9], which strongly affects the performance. The parameters of the virtual coupling were chosen to satisfy Llewellyn's stability criteria for human model parameters given in [10]. Fig. 13 shows left and right side of the Llewellyn's inequality. The system satisfies Llewellyn's stability criteria if the graph of left side of the Llewellyn's inequality (full bold line Fig. 13) exceeds the graph of right side of the Llewellyn's inequality. The Llewellyn's inequality and thus Llewellyn's stability criteria is satisfied for the model of the haptic display with human model (full line Fig. 13), but not for the model of the haptic display without the human model (dashed line, Fig. 13).

The main reasons for a discrepancy between simulation and experimental results regarding the frequency of oscillation are the following.

1) Mechanical coupling between joints. The actual haptic interface is a 6-DOF device, while a 1-DOF model simulates only the third joint. Preliminary experiments showed that the third joint contributes most to the amplitude of oscillations. Each joint has its own dynamics and, when coupled together, they form the combined endpoint dynamics of a 6-DOF haptic interface. The data presented in Figs. 9–11 result from combined dynamics, and the data presented in Figs. 5–7 show the results for a decoupled third joint.
2) Time variant and nonlinear dynamics of the overall hand grasp stiffness $H(s)$. A small range and slow movement of the haptic interface during the experiment were adopted, since it was shown that in such a case the linearized approximation is reasonable [11].

3) Temperature-dependence of the joint parameters. The robot was warmed up before starting the experiments.

For low values of stiffness k_e, the subject could penetrate a wall deeply enough to stay in the wall throughout the experiment, while, at high values of stiffness k_e, the wall penetration was inadequate. Hence, experiments for only low values of k_e [$k_e < 150\ \frac{\mathrm{N}}{\mathrm{m}}$, see Fig. 7(a)] were conducted, and the low level of stiffness had a negligible effect on the values of F_c and K_c.

Fig. 8 shows the simulation results for $k_e = [0{-}30000]\ \frac{\mathrm{N}}{\mathrm{m}}$. For high values, both the compensator filter ($k_e > 20000\ \frac{\mathrm{N}}{\mathrm{m}}$) and the virtual coupling ($k_e > 18000\ \frac{\mathrm{N}}{\mathrm{m}}$) have a destabilizing effect on the haptic interface. The literature on the stability analysis of high stiff walls [6], [14] gives a thorough insight into the solutions of problems related to sample-and-hold as well as sensor quantization, while we propose solutions on the basis of device dynamics.

B. Relation Between Human Arm Stiffness and Stability of the Haptic Interaction

Fig. 14 shows the simulated open-loop Bode plots of the haptic interaction for ideal ($G(s)H(s) = KY_e$), for the uncompensated system, for the compensated system, and for the system with virtual coupling. Biomechanical impedance of the human operator $H(s) = K$ does not affect the shape of the magnitude plot, but shifts it up or down by $20 \log_{10} K$. An ideal haptic interface is always stable, with phase always larger than -180°. The phase of an actual system drops below -180° for the uncompensated system, the compensated system, and the system with virtual coupling in the high-frequency region due to joint and PV controller dynamics, which introduce additional poles into the system. The added compensator filter damps the oscillating peak of the uncompensated system and increases the phase of the overall system in the critical frequency region. In addition, the interface transparency is improved, since the magnitude and phase of the compensated system are closer to ideal than in those of the uncompensated case (see Fig. 14). Similarly, the virtual coupling damps the oscillating peak and increases the phase of the overall system. However, on the basis of Fig. 14, it can be verified that the virtual coupling affects transparency considerably more than the compensator filter.

Since the exact relation between the grasp force and stiffness is not known, we present experimental results for the grasp force. However, higher grasp forces result in higher values of impedance [15], [16]. The overall hand grasp stiffness K combines both the stiffness of hand–arm and the stiffness of hand–handle coupling in a serial configuration [15]. Gurram *et al.* [8] proposed a linear relationship between stiffness and grasp force. The experimental data show a large increase of critical grasp force F_c at $m_e = 0.5$ kg and $b_e = 30\ \frac{\mathrm{N\,s}}{\mathrm{m}}$, indicating that the relationship between the grasp force and the hand grasp stiffness is not linear. The hand–handle coupling becomes stronger with increasing grasp force. Hand–handle coupling is dependent upon a superficial component of the flesh or skin of the palm and fingers, and upon a subcutaneous component of the flesh within the hand, which are all coupled to the motion of the handle [17].

A stiffer grasp results in higher human arm grasp stiffness K, which shifts the overall magnitude of the system up (Fig. 14)

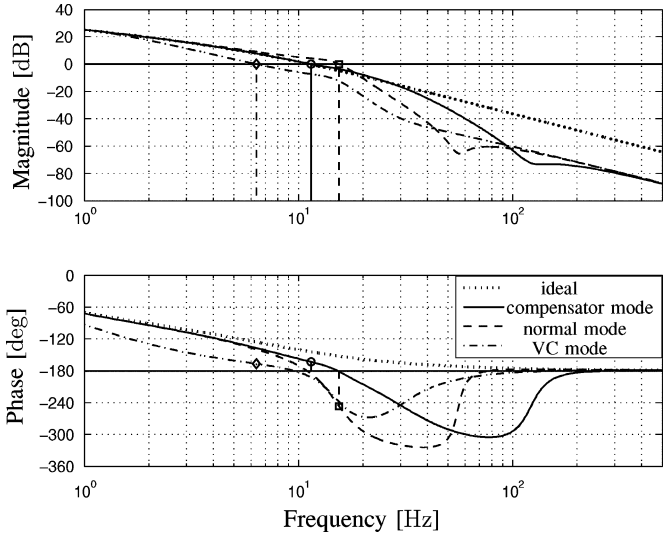

Fig. 14. Open-loop Bode plots of ideal (dotted line), uncompensated (broken line), compensated (solid line) haptic interface, and haptic system with virtual coupling (dash-dotted line). Circle indicates gain crossover frequency of compensated system, square representing the gain crossover frequency of uncompensated system, and diamond representing the gain crossover frequency of system with virtual coupling.

until the phase of the overall system at gain crossover frequency has reached -180°, which leads to the oscillations observed. The critical value of stiffness K_c is thus the value of K where the phase becomes -180°.

C. Concluding Remarks on the Use and Design of a Force-Filtering Compensator Filter

The design proposed in Section II-D has a number of similarities to the input-shaping techniques (IST) applied in industrial robotics for vibration reduction [18], and the loopshaping method for robust performance design.

The IST scheme utilizes a feedforward controller for suppressing vibrations and a feedback controller for attaining robustness against disturbances or parameter variations. Similarly, the approach proposed here uses the force-filtering compensator as a feedforward controller for preshaping force F_h in order to suppress the magnitude and to raise the phase in the resonant frequency region. The PV controller is used as a feedback controller.

The idea behind loopshaping is to construct an open-loop transfer function in such a manner that the feedback system is internally stable so that it satisfies the robust performance condition. Section II-D presents the procedure for C selection in such manner that $\widehat{Y}_e$ arbitrarily approximates Y_e by choosing the best performance values of ω_c and ζ_c.

For the best performance, the design of the compensator filter suggests values of ω_c frequency as high as possible. However, this will lead to a high attenuation $C(j\omega)|_{\omega \longrightarrow \infty} = \frac{\omega_c^2}{\omega_h^2}$ at high frequencies, which is not desirable. Tan *et al.* report that the upper bound of the human force control bandwidth is at about 7 Hz [19]. Hence, ω_c should at least match the haptic interface bandwidth and the human force control bandwidth. The compensator filter utilized has a simple design and can be implemented usefully, even if no strict identification of the

haptic interface has been made. On the basis of Figs. 9(b), 10(b), and 11(b), it can be resolved that the measured frequency of oscillation is always lower than the identified value of $\omega_h = 15$ Hz, and bandwidth should be chosen lower than the approximate value of ω_h to ensure a sufficient stability margin.

Last but not the least, a very important property of the proposed compensator filter is that it is not present in a feedback part of the control law framework, but is included in a feedforward chain. This enables a 2-DOF scheme where the prefilter and the feedback controller are obtained independently [20]. The proposed compensator filter can be combined with a number of known feedback algorithms for haptic interface control frameworks, such as algorithms for achieving passivity [12], [21].

V. Conclusion

The stability of a haptic interaction has been submitted to analysis, simulation, improvement, and experimental verification. A novel hand grasp force sensor setup was used to evaluate stability. Model analysis revealed that the main causes of instability are additional poles introduced by joint and PV controller dynamics, giving grounds for developing a control law for improving the stability of the haptic interaction. Analysis of critical grasp forces and critical values of human arm stiffness K_c showed that stability is highly dependent upon the stiffness of the human operator grasp. The results demonstrate that a higher grasp force and thus a higher hand grasp stiffness of the human arm require higher values of virtual mass and damping parameters of the virtual environment for the haptic interface to remain stable. A comparison of experimental and simulation results of an uncompensated system and a system with a compensator filter confirmed the improvement of stability. A comparison of the experimental results showed that the compensator filter performs better than virtual coupling. Evaluation of a model and experiments demonstrated that the critical grasp forces and the critical values of human arm stiffness displayed trends similar to the parameters of the virtual environment.

References

[1] R. J. Adams and B. Hannaford, "Stable haptic interaction with virtual environments," *IEEE Trans. Robot. Autom.*, vol. 15, no. 3, pp. 465–474, Jun. 1999.

[2] L. Clover, "A control-system architecture for robots used to simulate dynamic force and moment interaction between humans and virtual objects," *IEEE Trans. Syst., Man, Cybern. C, Appl. Rev.*, vol. 29, no. 4, pp. 481–493, Nov. 1999.

[3] N. Hogan, "Impedance control: An approach to manipulation, parts I–III," *J. Dyn. Syst. Meas. Control*, vol. 107, no. 1, pp. 1–24, Mar. 1985.

[4] J. E. Colgate and J. M. Brown, "Factors affecting the Z-width of a haptic display," in *Proc. IEEE Int. Conf. Robot. Autom.*, San Diego, CA, 1994, pp. 3205–3210.

[5] C. R. Carignan and K. R. Cleary. (2000, Feb.) Closed-loop force control for haptic simulation of virtual environments. *Haptics-e* [Online] *1(2)*. Available: http://www.haptics-e.org/.

[6] B. Gillespie and M. Cutkosky, "Stable user-specific haptic rendering of the virtual wall," in *Proc. ASME Int. Mech. Eng. Conf. Expo.*, 1996, pp. 397–406.

[7] J. L. Burke, R. R. Murphy, E. Rogers, V. J. Lumelsky, and J. Scholtz, "Final report for the DARPA/NSF interdisciplinary study on human–robot interaction," *IEEE Trans. Syst., Man, Cybern. C. Appl. Rev.*, vol. 34, no. 2, pp. 103–112, May 2004.

[8] R. Gurram, S. Rakheja, and G. J. Gouw, "Mechanical impedance of the human hand-arm system subject to sinusoidal and stochastic excitations," *Int. J. Ind. Ergon.*, vol. 16, no. 2, pp. 135–145, Aug. 1995.

[9] R. J. Adams and B. Hannaford, "Control law design for haptic interfaces to virtual reality," *IEEE Trans. Control Syst. Technol.*, vol. 10, no. 1, pp. 3–13, Jan. 2002.

[10] D. J. Bennett, J. M. Hollerbach, Y. Xu, and I. W. Hunter, "Time-varying stiffness of human elbow joint during cyclic voluntary movement," *Exp. Brain Res.*, vol. 88, no. 2, pp. 433–442, Feb. 1992.

[11] A. J. Hodgson and N. Hogan, "A model-independent definition of attractor behavior applicable to interactive tasks," *IEEE Trans. Syst., Man, Cybern. C, Appl. Rev.*, vol. 30, no. 1, pp. 105–118, Feb. 2000.

[12] B. Hannaford and J. H. Ryu, "Time domain passivity control of haptic interfaces," *IEEE Trans. Robot. Autom.*, vol. 18, no. 1, pp. 1–10, Feb. 2002.

[13] R. W. McGorry, "A system for the measurement of grip forces and applied moments during hand tool use," *Appl. Ergon.*, vol. 32, no. 3, pp. 271–279, Jun. 2001.

[14] J. E. Colgate, M. C. Stanley, and J. M. Brown, "Issues in the haptic display of tool use," in *Proc. IEEE/RSJ Int. Conf. Intell. Robot. Syst.*, Pittsburgh, PA, 1995, vol. 3, pp. 140–145.

[15] F. C. T. van der Helm, A. C. Schouten, E. de Vlugt, and G. G. Brouwn, "Identification of intrinsic and reflexive components of human arm dynamics during postural control," *J. Neurosci. Methods*, vol. 119, no. 1, pp. 1–14, Sep. 2002.

[16] Z. Jandak, "Driving-point mechanical impedance of the hand-arm system at exposure to stochastic vibration," in *Proc. Int. Conf. Hand-Arm Vib.*, Umea, Sweden, 1998, pp. 11–12.

[17] R. Gurram, S. Rakheja, and A. J. Brammer, "Driving-point mechanical impedance of the human hand-arm system: Synthesis and model development," *J. Sound Vib.*, vol. 180, no. 3, pp. 437–458, 1995.

[18] P. H. Changa and H.-S. Park, "Time-varying input shaping technique applied to vibration reduction of an industrial robot," *Control Eng. Pract.*, vol. 13, no. 1, pp. 121–130, Jan. 2005.

[19] H. Z. Tan, M. A. Srinivasan, B. Ebermann, and B. Cheng, "Human factors for the design of force-reflecting haptic interfaces," *Dyn. Syst. Control*, vol. 55, no. 1, pp. 353–359, 1994.

[20] I. Yaesh and U. Shaked, "Two-degree-of-freedom H-optimization of multivariable feedback systems," *IEEE Trans. Autom. Control*, vol. 36, no. 11, pp. 1272–1276, Nov. 1991.

[21] M. Mahvash and V. Hayward, "High fidelity passive force reflecting virtual environments," *IEEE Trans. Robot.*, vol. 21, no. 1, pp. 38–46, Feb. 2005.

Janez Podobnik received the University Degree in electrical engineering in 2004 from the University of Ljubljana, Ljubljana, Slovenia, where he is currently working toward the Ph.D. degree.

He is currently a Teaching Assistant in the Laboratory of Robotics and Biomedical Engineering, Faculty of Electrical Engineering, University of Ljubljana. His current research interests include haptic interfaces and real-time control of haptic devices and robots for virtual reality-supported hand rehabilitation.

Marko Munih (M'88) received the B.Sc., M.Sc., and D.Sc. degrees in electrical engineering from the University of Ljubljana, Ljubljana, Slovenia, in 1986, 1989, and 1993, respectively.

In 1989, he was a Teaching Assistant and, in 1997, an Assistant Professor in the Faculty of Electrical Engineering, University of Ljubljana. From 1995 to 1996, he was a Research Assistant in the Implanted Devices Group, Department of Medical Physics and Bioengineering, University College London, London, U.K. and Royal National Orthopaedic Hospital Trust, Stanmore, U.K. His current research interests include functional electrical stimulation of paraplegic lower extremities with surface electrode systems, including measurements, control, biomechanics, and electrical circuits. Currently, he is a Professor and Head of the Laboratory of Robotics and Biomedical Engineering, Faculty of Electrical Engineering, University of Ljubljana.

Dr. Munih is a member of the International Federation for Medical and Biological Engineering, the International Functional Electrical Stimulation Society, and the International Federation of Automatic Control. He was the recipient of the Zois Award in 2002.